Air-coupled method to investigate the lowest-order antisymmetric Lamb mode in stubbed and air-drilled phononic platess

Dongbo Zhang, Jinfeng Zhao, Bernard Bonello, Libing Li, Jianxin Wei, Yongdong Pan, Zheng Zhong

Air-coupled method to investigate the lowest-order antisymmetric Lamb mode in stubbed and air-drilled phononic plates

Dongbo Zhang, Jinfeng Zhao, Bernard Bonello, Libing Li, Jianxin Wei, Yongdong Pan, and Zheng Zhong

Citation: AIP Advances **6**, 085021 (2016); doi: 10.1063/1.4962222
View online: http://dx.doi.org/10.1063/1.4962222
View Table of Contents: http://scitation.aip.org/content/aip/journal/adva/6/8?ver=pdfcov
Published by the AIP Publishing

Air-coupled method to investigate the lowest-order antisymmetric Lamb mode in stubbed and air-drilled phononic plates

Dongbo Zhang,[1] Jinfeng Zhao,[1,a] Bernard Bonello,[2] Libing Li,[1] Jianxin Wei,[3] Yongdong Pan,[1] and Zheng Zhong[1]
[1]*School of Aerospace Engineering and Applied Mechanics, Tongji University, 100 Zhangwu Road, 200092, Shanghai, China*
[2]*CNRS, UMR 7588, Institut des NanoSciences de Paris, F-75005, Paris, France*
[3]*State Key Laboratory of Petroleum Resources and Prospecting, China University of Petroleum, 18 Xuefu Road, 102249, Pekin, China*

(Received 1 July 2016; accepted 22 August 2016; published online 30 August 2016)

In this work, we applied a robust and fully air-coupled method to investigate the propagation of the lowest-order antisymmetric Lamb (A_0) mode in both a stubbed and an air-drilled phononic-crystal (PC) plate. By measuring simply the radiative acoustic waves of A_0 mode close to the plate surface, we observed the band gaps for the stubbed PC plate caused by either the local resonance or the Bragg scattering, in frequency ranges in good agreement with theoretical predictions. We measured then the complete band gap of A_0 mode for the air-drilled PC plate, in good agreement with the band structures. Finally, we compared the measurements made using the air-coupled method with those obtained by the laser ultrasonic technique.
[http://dx.doi.org/10.1063/1.4962222]

I. INTRODUCTION

As a result of their periodicity, phononic crystals (PC's) exhibit absolute band gaps, *i.e.* frequency regions over which the propagation of elastic waves is forbidden whatever the incident direction. These Bragg gaps, that open up at the Brillouin zone (BZ) boundaries when the wavelength is comparable to the period, originate from the destructive interferences that the waves undergo when they are multiply scattered by the periodic array of inclusions.[1–5] Another type of gap originating from a distinct physical process can also appear in the dispersion curves when the scatters behave like local resonators. These gaps are not related to the periodicity of the medium and hence, they may open up at frequencies much lower than the Bragg gaps.[6–11] This has been observed and investigated, for instance, for Lamb waves propagating in a plate with stubbed structures,[11–15] whereas only the Bragg mechanism occurs in a PC made of air holes drilled through the plate.[4,5]

In practice, these hetero-structures are generally placed in the air which, because of its extremely low acoustic impedance, does not play any role in the calculation of the band structure. Therefore, the coupling effects between the acoustic waves in the air medium and the elastic modes in the solid structure are seldom included in the physical models, except in very specific investigations such as those aiming at solving some computation difficulties.[16–18] Indeed, when using the subwavelength structure to control the propagation of sound for either the super-transmission[19,20] or the super-absorption,[21–24] the possible influence of leaky Lamb modes in the solid structure on the sound propagation in the air medium has been noticed. However, this coupling effect which occurs at oblique incidence, was generally not investigated in former studies where only the normal

[a]Authors to whom correspondence should be addressed. Electronic addresses: jinfeng.zhao@tongji.edu.cn

incidence is considered. The reverse process, *i.e.* using the sound wave in the air medium to control or to measure the Lamb waves in a periodic solid structure, has remained almost unexplored to date.

Likewise, the experimental evidence of band gaps is usually obtained by means of piezoelectric transducers or using the laser ultrasonic technique,[12–15] while to date none experiment has been achieved using the air-coupled method. Actually, recent progresses made in the field of the nondestructive evaluation (NDE) techniques allowed for the development of air-coupled transducers (ACT's) both to generate and to detect Lamb waves in composite plates,[25] with the advantage over more conventional methods of the absence of any contact and an even higher efficiency. Hybrid methods, involving an ACT for the excitation in conjunction with a laser Doppler vibrometer (LDV) for the detection, have also been employed to investigate the dispersion of the lowest-order Lamb (A_0) mode in metallic or composite plates.[26–28]

In view of the importance of studying the dispersion of Lamb waves in PC's and based on these technical progresses, we have investigated the propagation of A_0 mode either in a stubbed and or in an air-drilled PC plate using ACT's as emitter and receiver. We report on the transmission spectra and the acoustic field in both samples for frequencies in or out the first two band gaps. At last, we compare the measurements made by using either the air-coupled method or the laser ultrasonic technique.

II. EXPERIMENTAL SETUP

The experimental configuration is shown in Figure 1. Two unfocused ACT's were used as emitter and receiver respectively. The ACT's feature a transitional layer matched to the air medium to reduce significantly the signal losses.[25–28] The emitter was adjusted in the x-z plane at an angle θ to the z-axis. It was attached to a high power generator (JPR-600C – electric potential of 600 V) delivering five-cycles sinusoidal acoustic pulses windowed by a Hanning function, at a repetition rate of 500 Hz. These pulses impinged the homogeneous plate over an area comparable to the surface of the ACT, just a few centimeters in front of the PC. The sample was attached to a two-axis translation stage allowing for motions in the x-y plane. A recursive algorithm allowed to compute the dispersion of the Lamb modes in the homogeneous plate and in turn to deduce their slowness s_x along the x-axis. Indeed, the Snell's law relates s_x and the incident angle θ through the relationship $\theta = \sin^{-1}(s_x \cdot c)$ where c is the sound velocity in the air medium.[29]

By setting the incident angle θ to the position where the dispersion of A_0 mode of the homogeneous plate exists at the given frequency, the Gaussian profile collimated wave pulses sent from the circular surfaces of ACTs produces an ellipse-shaped excitation region on the surface of plate.

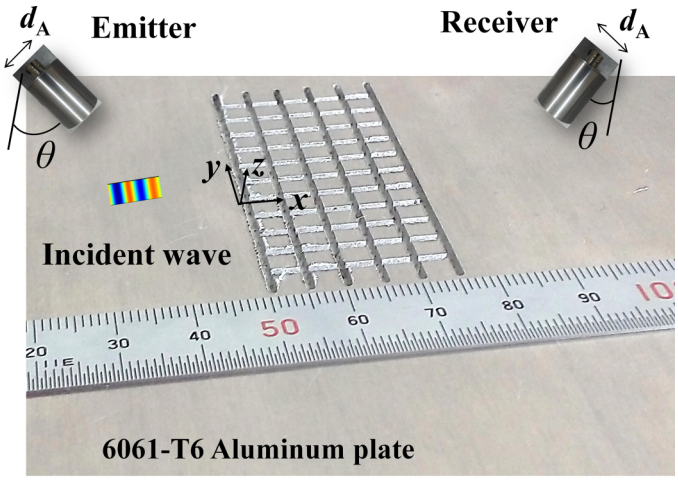

FIG. 1. Experimental configuration: acoustic pulses issuing from the ACT emitter impinge the plate and generate A_0 mode, while the ACT receiver records the radiative waves created in the air background by A_0 mode. The stubbed PC plate features the lattice constant a=5 mm. The diameter d_A of ACT used in this work is between 27 and 46 mm.

As a result, A_0 mode is generated within the ellipse-shaped region with the Gaussian amplitude profile along the y-axis.[27–29] As the A_0 mode propagates along the plate, the waist of the Gaussian profile increases gradually. In the far field, our measurement shows that the A_0 mode occupies approximately a 90° fan-shaped region with the symmetric axis parallel to the x-axis and the apex overlapped to the center of the ellipse-shaped excitation region. The incident A_0 mode pulses to the PC plate located far away from the excitation region can therefore be treated as normally incident plane waves. The detection of Lamb wave results from the reciprocal physical process. The A_0 mode acts as a source which radiates acoustic pulses into the adjacent air media. These acoustic waves are recorded by the receiver above the sample and further amplified by a preamplifier (60 dB). This large pre-amplification is necessary since the original signal of the radiative wave pulses of the A_0 mode into the air media is very small in comparison to the incident wave pulses issued directly from the emitter ACT, for the strong losses caused by the huge impedance mismatch between the air and the solid media. The acquired signals were then digitized by an oscilloscope (DPO 4102B-L) at the sampling rate of 50 MHz. Up to 32 scans were averaged to get a very good signal to noise (S/N) ratio. Both the emitter and the receiver were positioned at the same distance off the plate along the z-axis; a narrow sponge extending a few centimeters along the z-axis was glued on the plate in between the emitter and the receiver to prevent the measurement chain from the air disturbance. Different pairs of ACT's, hereafter referred to as ACT 1, 2 and 3, were used to sweep the frequency range. Their respective central frequency was 50, 190, and 420 kHz, the bandwidth was 40%, 15%, and 18%, the diameter was 46, 32, and 27 mm; the optimal incidence angles were respectively equal to 17.45°, 10.15° and 8.15° for the 3 mm thick homogeneous 6061-T6 aluminum plate used in this work.

To show how efficient is the air-coupled method, we first made measurements on a 3 mm thick homogeneous 6061-T6 aluminum plate by using the ACT 2 transducers. The mass density and elastic constants of aluminum used in this work are ρ=2700 kg·m^{-3}, C_{11}=111 GPa, C_{12}=61 GPa, C_{44}=25 GPa, respectively. The measurements were made every 1.26 mm, over a distance of ~103 mm along the x-axis, starting ~50 mm behind the emitter. Figure 2 shows the normalized component of the two-dimensional (2D) Fourier transform of the recorded signals together with the dispersion curves (white dotted lines) of the A_0 mode, the zero-order symmetric Lamb (S_0) mode, and the first-order antisymmetric Lamb (A_1) mode. Unambiguously, the data centered at 190 kHz well spread along the branch of the A_0 mode, demonstrating the accuracy of this device for both the excitation and the measurement of A_0 mode. However, we presented in this work no

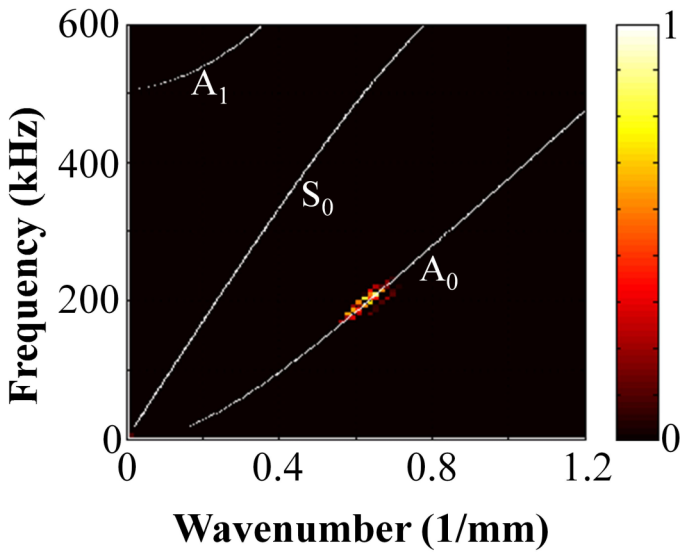

FIG. 2. Two-dimensional Fourier transform of the signals measured along a line on the homogeneous plate 3 mm in thickness, using the pair of ACT2.

relevant investigations on any other Lamb modes to focus our attention on the A_0 mode for its wide applications in the NDE, sensors, etc.

III. STUBBED STRUCTURE AND RESULTS

The stubbed PC plate consisted of a periodic arrangement of 5×12 square shaped pillars with the square symmetry and a lattice parameter equal to a=5 mm, obtained by digging equidistant channels on a 6061-T6 aluminum plate (see Fig. 1). The height and the width of the pillars were h_1=2 and b=3.6 mm respectively; the thickness of the plate was h_2=1 mm.

We used a finite element method (FEM) (COMSOL Multiphysics) to compute the band structure along the direction ΓX of the BZ. Two forbidden bands, emphasized by the gray areas in Fig. 3(a), open up in between [161, 206] and [326, 383] kHz respectively along the ΓX. We further computed the transmission through the five unit cells of the PC shown in Fig. 1, when A_0 mode propagates along the x-axis.[30,31] The surrounding air was not considered in the numerical model to save the computation cost and to guarantee the computation accuracy. Computation details are given in Ref. 31. The transmission coefficient, defined as $T = 10\log\left(u_z/u_{z_0}\right)$, is shown as a function of frequency in Fig. 3(b). In the definition of T, u_z and u_{z_0} stand for the out-of-plane amplitude of the transmitted and incident waves respectively. Two forbidden bands satisfying $T < -30$ dB are observable in Fig. 3(b): the first one falls in the interval [160, 201] kHz, in good agreement with the first band gap in Fig. 3(a). The second stop band in between 319 and 447 kHz is above and broader than expected from the dispersion curves in Fig. 3(a). While the calculated lower edge of this gap is in good agreement with the dispersion curves, the enlargement towards the upper edge (447 kHz instead of 383 kHz) has a major origin. Actually, in the frequency range [383, 447] kHz the dispersion curves feature a single mode composed of the first-order shear-horizontal Lamb (SH_1) mode of the substrate plate and one bending vibration of the pillar, as noted by the red line in Fig. 3(a). Since the displacement field of the substrate plate is dominated by u_y, this hybrid mode cannot be excited by the A_0 mode created in the homogeneous plate so that the incident wave propagates into the narrow channels in between the pillars as what happens in the second stop band (see below). Therefore destructive interferences are formed, and T falls below −30 dB.

Then, we measured the transmission coefficient piecewise, using the three ACT's described above. The experiments were conducted in the linear regime and therefore the recorded signals were proportional to the out-of-plane displacement, allowing for a direct comparison with the numerical simulation. The results are summarized in Fig. 3(c) as black, red, and blue lines according to the

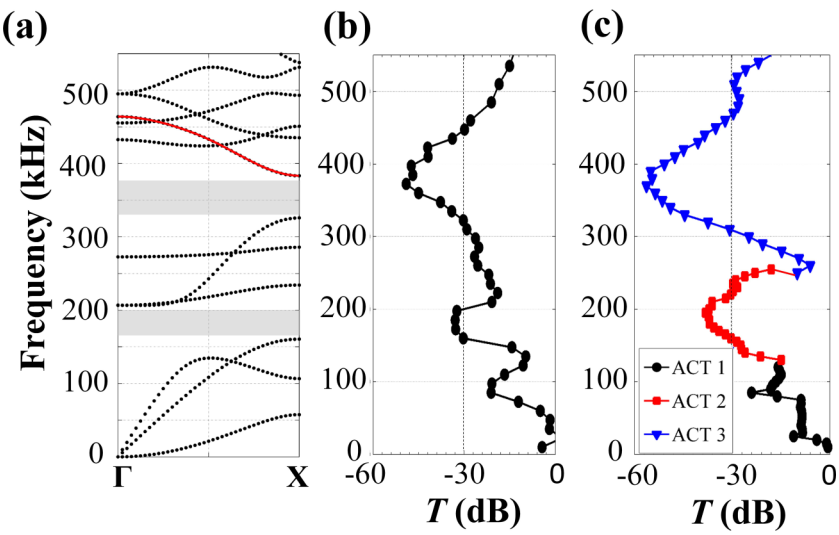

FIG. 3. (a) Band structures of stubbed PC made of square pillars with a width b=3.6 mm and a thickness h_2=2 mm erected on the 1 mm thick plate. The lattice had the square symmetry featuring the lattice constant a=5 mm; (b) calculated and (c) measured transmission spectra of A_0 mode.

frequency range of each pair of ACT's. Fig. 3(c) shows two forbidden bands where T is below −30 dB: the first one falls in the interval [159, 223] kHz, in good agreement with the low frequency band gap in Figs. 3(a) and 3(b), while the second one that stretches in between 309 and 467 kHz, is larger as compared with the second band gap in Fig. 3(b). This discrepancy must be ascribed to the characteristic of the transmission in the second band. As noted in Fig. 3(b), T is very close to −30 dB over relatively broad regions at both the upper and the lower edges of the second stop band. These slow variations of T cannot be fully reproduced in experiments because of some limited specifications of the ACT's (bandwidth, rise time…). So that experimentally, a broader stop band is observed in the high frequency range. Nevertheless, the radiative modes attenuate as does the A_0 mode within the band gaps of the stubbed structure, and this feature is clearly reproduced by our air-coupled experimental method.

Whether in experiment or in simulation, the second band gap we observed is much deeper than its low frequency counterpart. To further illustrate this, we have performed another experiment where the sample was rotated 90° in the x-y plane and all other conditions kept unchanged. That is to say the stubbed PC plate consisted of 12 rows of square pillars along the x-axis. Fig. 4(a) shows T measured inside the stubbed PC along the propagation direction at 50 (black line), 200 (red line), and 400 kHz (blue line), respectively. At 50 kHz, T decreases gradually along the x-axis due to internal reflection and diffusion processes in the PC plate, but never falls below −20 dB. Within the forbidden bands, T decreases exponentially down to −30 dB at x=6a for 200 kHz or at x=4a for 400 kHz, clearly displaying a larger damping rate at the higher frequency. This difference in the damping rates can be attributed to the mechanisms responsible for the two band gaps that are pointed out by the normalized out-of-plane displacement field at 200 and 400 kHz, computed using the numerical method described in Ref. 30 (see Fig. 4(b)). At 200 kHz, the energy is localized in the pillar so that the band gap must be attributed to a local resonance (a flexural resonance here) of the pillars in the PC. In the present case, both the pillars and the substrate being made of aluminum, the coupling between the substrate and the resonator is good, and consequently the elastic energy cannot get confined in the resonators for a long time. This explains also why a deep gap is not observed at 200 kHz in Figs. 3(a) and 3(b). The situation is somehow different at 400 kHz. Actually, around this frequency the elastic energy gets concentrated in the plate, and therefore the band gap must be ascribed to the interferences between the different lines of pillars, *i.e.* to the Bragg mechanism. Accordingly, the second band gap results from a stronger damping of the waves and features therefore a larger depth.

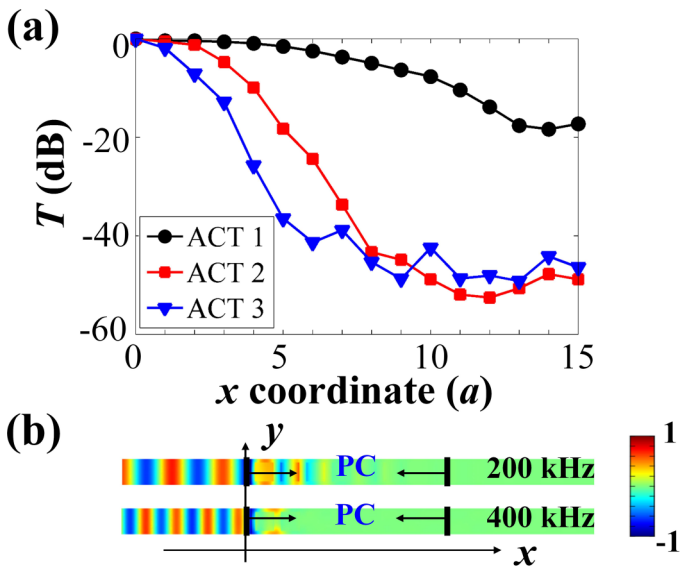

FIG. 4. (a) Experimental transmission coefficient T measured downstream the stubbed PC plate at 50 (black), 200 (red), and 400 kHz (blue); (b) normalized displacement field of u_z calculated by FEM at 200 and 400 kHz.

IV. AIR-DRILLED STRUCTURE AND RESULTS

There is another representative type of PC's in which measuring the band gaps thanks to the radiative waves in the air medium surrounding the structure is very interesting. These are PC's constituted of air holes drilled throughout a plate. To show that, arrays of air holes in honeycomb lattice with a diameter d_a=4.20 mm and a lattice constant a=4.62 mm, were drilled throughout a 6061-T6 aluminum plate of 3 mm in thickness. By means of a machining process, we fabricated the sample on a 56×57 mm^2 area as shown by the inset in Fig. 5(a). Upon completion, random disorder on the diameter of the air holes d_a was observed to follow the distribution $d_a = d_{a0}\left[1+\sqrt{3}\delta\,(2\beta-1)\right]$,[32] where the standard uniformly distributed random variable $\beta \in (0,1)$, and the disorder coefficient δ was less than 0.02. The mean diameter of the air holes d_{a0} measured on each side of the plate was 4.19 and 4.17 mm, respectively.

The band structures of the designed PC plate that we show in Fig. 5(a) features a large complete band gap caused by the Bragg mechanism within the frequency range [197, 251] kHz. Fig. 5(b) shows the transmission coefficient T measured along ΓK using either ACT 1 (black line) or ACT 2 (red line). The band gap stretches over the frequency range [204, 257] kHz in very good agreement with the computations shown in Fig. 5(a). Therefore, the disorder has almost no influence neither on the position nor on the width of the band gap, in accordance with previous works[15,30] where the influence of a small variance δ on the band gaps was investigated. Fig. 5(c) shows the variations of T along ΓM and brings to light a band gap in the range [178, 265] kHz slightly larger than the one measured along ΓK. This can be ascribed to the difference in the paths along ΓK and ΓM. Actually, in a microscopic view, along the ΓM direction, the waves go through one type of the narrow bridges between two air holes in the direction perpendicular to the axis through the centers of these two adjacent air holes (see inset in Fig. 5(c)), and the bridges behave then like local resonators that stores elastic energy. This does not happen for the propagation along ΓK (see inset in Fig. 5(b)), so that the transmission coefficient T shall be smaller along the ΓM as it is actually observed in Figs. 5(b) and 5(c). In return, close the edges of the band gap, T falls below −30 dB and the width is a little enlarged. Therefore, the radiative waves transmitted in the air medium accurately reflect the band gaps of Lamb modes in air-drilled PC plate.

The agreement between the transmission spectra measured by ACT's and the theoretical ranges of the stop bands must also be ascribed to the fact that the wavelength in the air medium λ is much smaller than the periodic constant for both structures, either at 200 kHz ($\lambda \approx 1.72$ mm) or at

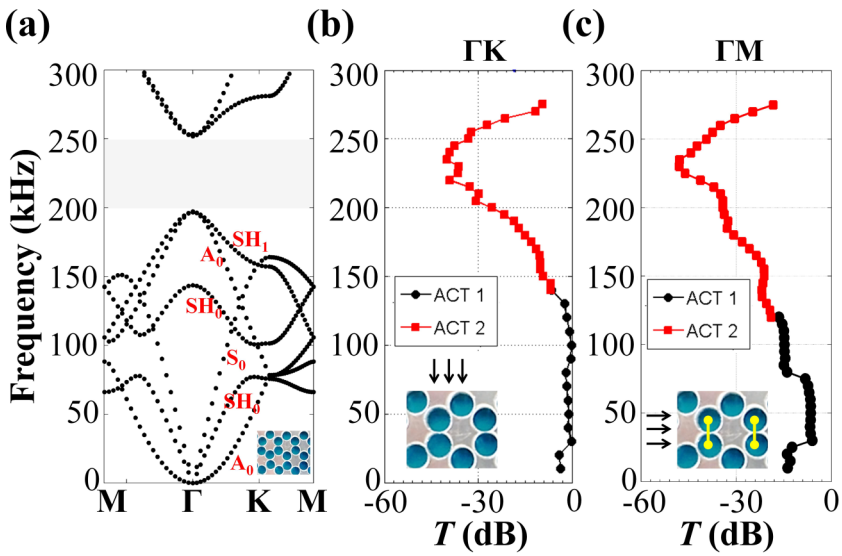

FIG. 5. (a) Band structure of the air-drilled honeycomb PC plate (inset) with the lattice constant a=4.62 mm, the diameter of the air holes d_a=4.2 mm, and the plate thickness h=3 mm; measured transmission coefficient along the (b) ΓK and (c) ΓM direction.

400 kHz ($\lambda \approx 0.86$ mm). This is quite different from previous studies which focused on using the resonant modes of periodic structure in the long-wavelength regime.[19–24]

V. COMPARISON BETWEEN MEASUREMENTS BY ACT AND LDV

In this section we compare the respective achievements of the ACT and the LDV which was used as receiver to measure the out-of-plane displacements of the A_0 Lamb mode with a frequency of 180 kHz, after they propagate along a fixed distance ~14 cm in a 3 mm thick 6061-T6 aluminum plate free of any inclusions. In both cases, we used the ACT 2 to excite the Lamb wave. For the measurements with the ACT, we used our former experimental setup and, when using the LDV (*i.e.* Polytec vibrometer OFV 2570), a similar experimental setup as the one described in Refs. 27 and 28.

Figure 6 shows the normalized power recorded by using either the ACT receiver (square markers) or the LDV (circular markers) against the electrical potential applied on the ACT emitter. We can see that the signal delivered by the ACT receiver is proportional to the electrical potential applied to the emitter. On the other hand, the LDV yields a quasilinear profile with fluctuations that must be ascribed to the fluctuations of the contrast of the interference pattern in LDV resulting from the environmental noise. Clearly, the air-coupled method features over LDV device a more robust advantage against the environmental fluctuations. This can be easily understood since the LDV measures a small spot on the plate so that it allows for a high spatial resolution but it is sensitive to noise. The ACT records signals within a large area, and therefore the environmental noise (white noise) is averaged at the sacrifice of the spatial resolution. For the extremely low electrical potential of 20 V, the measured S/N ratio is less than 2 when using the LDV but it is more than 10 if using the ACT. This demonstrates the stable performance of ACT for the very small out-of-plane displacement as compared to the LDV, opening a way to use in the future the ACT to the measurement of Lamb waves at micrometer scale, for example in the MEMS systems, with the availability of high performance ACTs designed for this spatial scale.

VI. CONCLUSIONS

In summary, we reported on the propagation of A_0 mode in PCs plates measured by using the fully air-coupled method. We investigated first, both numerically and experimentally, the transmission spectra and the field distribution in a stubbed PC plate, showing the existence of two forbidden bands due to the local resonance of inclusions at low frequency and to the Bragg scattering at high

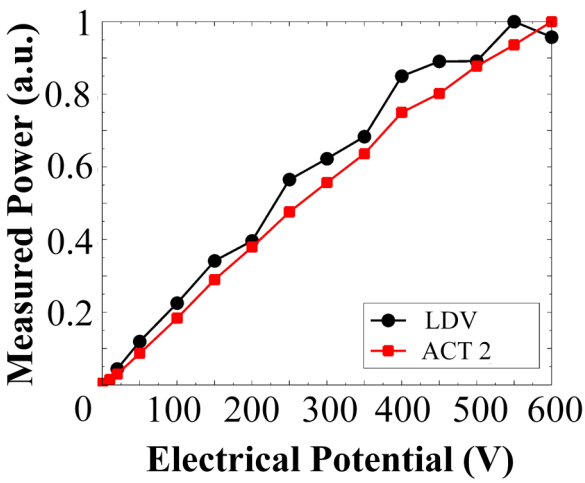

FIG. 6. Measured power by using the LDV (circular markers) and ACT (square markers) against the applied electrical potential on ACT2 emitter for 180 kHz.

frequency. The attenuation of A_0 mode leads to a deeper band gap in the high frequency forbidden band. We studied then the complete band gap due to Bragg scatterings in an air-drilled PC plate with small disorder which has almost no influence on the frequency range of the complete band gap. We found differences in the transmission along different directions in the BZ of the air-drilled PC plate. At last, we compared the measurements made by using the air-coupled technology and by the laser ultrasonic technique. The air-coupled method can be extended in future to the measurement of energy absorption or to the micrometer scaled samples.

ACKNOWLEDGEMENTS

This work was supported by the National Natural Science Foundation of China under Grant No. 11602174.

[1] M. S. Kushwaha, P. Halevi, L. Dobrzynski, and B. Djafari-Rouhani, Phys. Rev. Lett. **71**, 2022 (1993).
[2] J. O. Vasseur, P. A. Deymier, B. Chenni, B. Djafari-Rouhani, L. Dobrzynski, and D. Prevost, Phys. Rev. Lett. **86**, 3012 (2001).
[3] B. Bonello, C. Charles, and F. Ganot, Appl. Phys. Lett. **90**, 021909 (2007).
[4] X. Zhang, T. Jackson, E. Lafond, P. Deymier, and J. Vasseur, Appl. Phys. Lett. **88**, 041911 (2006).
[5] S. Mohammadi, A. A. Eftekhar, A. Khelif, W. D. Hunt, and A. Adibi, Appl. Phys. Lett. **92**, 221905 (2008).
[6] Z. Liu, X. Zhang, Y. Mao, Y. Y. Zhu, Z. Yang, C. T. Chan, and P. Sheng, Science **289**, 1734 (2000).
[7] M. Hirsekorn, P. P. Delsanto, A. C. Leung, and P. Matic, J. Appl. Phys. **99**, 124912 (2006).
[8] W. Xiao, G. W. Zeng, and Y. S. Cheng, Appl. Acoust. **69**, 255 (2008).
[9] J.-C. Hsu and T.-T. Wu, Appl. Phys. Lett. **90**, 201904 (2007).
[10] J.-H. Sun and T.-T. Wu, Phys. Rev. B **76**, 104304 (2007).
[11] Y. Pennec, B. Djafari-Rouhani, H. Larabi, J. O. Vasseur, and A. C. Hladky-Hennion, Phys. Rev. B **78**, 104105 (2008).
[12] T.-T. Wu, Z.-G. Huang, T.-C. Tsai, and T.-C. Wu, Appl. Phys. Lett. **93**, 111902 (2008).
[13] T.-C. Wu, T.-T. Wu, and J.-C. Hsu, Phys. Rev. B **79**, 104306 (2009).
[14] M. Oudich, M. Senesi, M. B. Assouar, M. Ruzenne, J.-H. Sun, B. Vincent, Z. Hou, and T.-T. Wu, Phys. Rev. B **84**, 165136 (2011).
[15] M. Rupin, F. Lemoult, G. Lerosey, and P. Roux, Phys. Rev. Lett. **112**, 234301 (2014).
[16] J. O. Vasseur, P. A. Deymier, A. Khelif, Ph. Lambin, B. Djafari-Rouhani, A. Akjouj, L. Dobrzynski, N. Fettouhi, and J. Zemmouri, Phys. Rev. E **65**, 056608 (2002).
[17] R. Sainidou, B. Djafari-Rouhani, Y. Pennec, and J. O. Vasseur, Phys. Rev. B **73**, 024302 (2006).
[18] J. O. Vasseur, P. A. Deymier, B. Djafari-Rouhani, Y. Pennec, and A-C. Hladky-Hennion, Phys. Rev. B **77**, 085415 (2008).
[19] H. Estrada, P. Candelas, A. Uris, F. Belmar, F. J. Garíca de Abajo, and F. Meseguer, Phys. Rev. Lett. **101**, 084302 (2008).
[20] F. Liu, F. Cai, Y. Ding, and Z. Liu, Appl. Phys. Lett. **92**, 103504 (2008).
[21] J. Christensen, V. Romero-García, R. Picó, A. Cebrecos, F. J. García de Abajo, N. A. Mortensen, M. Willatzen, and V. J. Sánchez-Morcillo, Sci. Rep. **4**, 4674 (2014).
[22] M. Yang, C. Meng, C. Fu, Y. Li, Z. Yang, and P. Sheng, Appl. Phys. Lett. **107**, 104104 (2015).
[23] V. Leroy, A. Strybulevych, M. Lanoy, F. Lemoult, A. Tourin, and J. H. Page, Phys. Rev. B **91**, 020301(R) (2015).
[24] Y. Li and B. M. Assouar, Appl. Phys. Lett. **108**, 063502 (2016).
[25] M. Garcia-Rodriguez, Y. Yañez, M. J. Garcia-Hernandez, J. Salazar, A. Turo, and J. A. Chavez, J. Nondestruct. Eval. **30**, 50 (2011).
[26] Z. Liu, H. Yu, C. He, and B. Wu, Phys. Mech. & Astr. **56**, 7 (2013).
[27] M. S. Harb and F. G. Yuan, Ultrasonics **61**, 1 (2015).
[28] M. S. Harb and F. G. Yuan, Ultrasonics **64**, 162 (2016).
[29] J. Zhao, Y. Pan, and Z. Zhong, J. Appl. Phys. **113**, 054903 (2013).
[30] A. Khelif, S. Mohammadi, A. A. Eftekhar, A. Adibi, and B. Aoubiza, J. Appl. Phys. **108**, 084515 (2010).
[31] J. Zhao, B. Bonello, and O. Boyko, AIP Advances **4**, 124204 (2014).
[32] Z.-Z. Yan, C. Zhang, and Y.-S. Wang, Wave Motion **47**, 409 (2010).